Earth, Planets and Space

FULL PAPER Open Access

Ionospheric signatures of repeated passages of atmospheric waves by the 2022 Jan. 15 Hunga Tonga-Hunga Ha'apai eruption detected by QZSS-TEC observations in Japan

Kosuke Heki[1,2*]

Abstract

A large eruption occurred on Jan. 15, 2022, at the submarine volcano Hunga Tonga-Hunga Ha'apai, southern Pacific, and the atmospheric Lamb wave was observed to have traveled round the Earth multiple times with a speed of ~ 0.3 km/s. Here, I compare their ionospheric and atmospheric signatures using data from dense arrays of barometers and GNSS stations in Japan. I confirmed that the ionospheric disturbances passed over Japan at least four times, first from SE to NW, then from NW to SE, again from SE to NW, and finally from NW to SE. The propagation velocity of the ionospheric disturbances was as fast as the atmospheric Lamb wave, suggesting their origin as upward energy leakage from the troposphere. The first passage of the ionospheric disturbance started prior to the arrival of the Lamb pulse, but its physical mechanism is yet to be explored. Unlike the barometric records, waveforms and amplitudes of ionospheric disturbances exhibit large diversity along the wavefront, suggesting their turbulent nature.

Keywords: QZSS, GNSS, Ionospheric disturbance, Total electron content, Hunga Tonga-Hunga Ha'apai, Lamb wave

*Correspondence: heki@sci.hokudai.ac.jp

[1] Shanghai Astronomical Observatory, Chinese Academy of Sciences, 80 Nandan Rd., Shanghai 200030, China
Full list of author information is available at the end of the article

Graphical Abstract

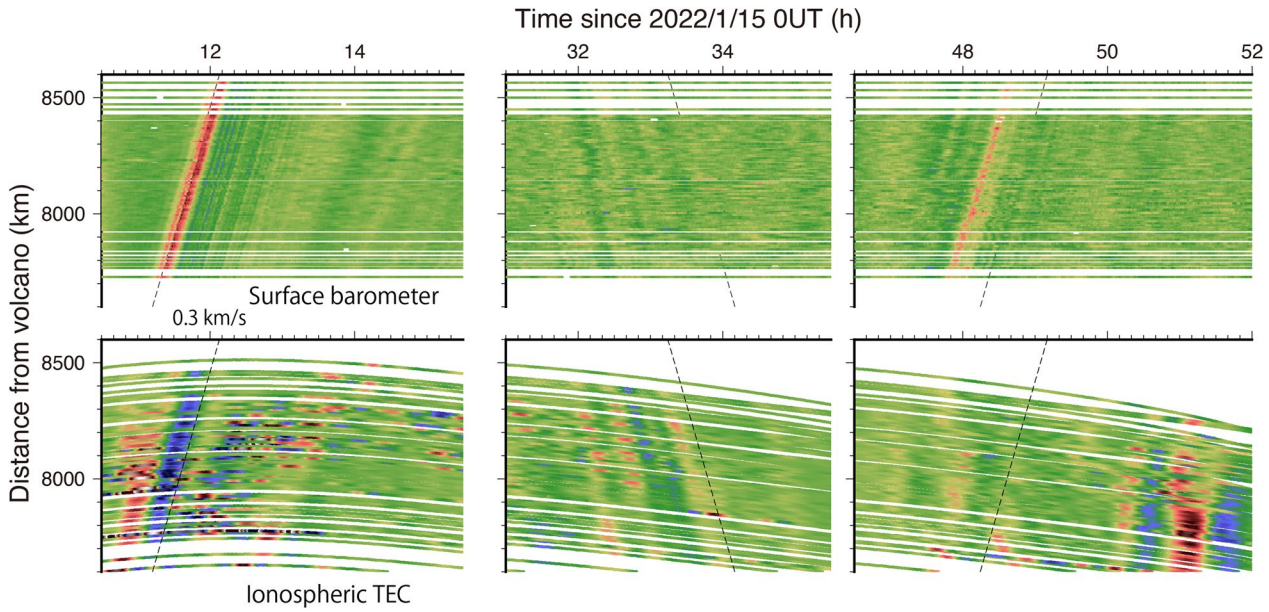

Introduction

A strong eruption with the volcanic explosivity index (VEI) 5, started at the Hunga Tonga-Hunga Ha'apai submarine volcano, South Pacific, at ~ 04:15 UT, on 15 Jan. 2022. About 7 h after the eruption, a dense array of atmospheric barometers in Japan, ~ 8000 km away from the volcano, detected the passages of the atmospheric wave from SE to NW as a positive pulse of pressure of a few hPa (Weathernews 2022). This wave seems to have traveled along the great circle from the volcano with the speed of ~ 0.3 km/s. Following this first passage along the short-path, the second passage from NW to SE along the long-path was identified. Infrasound sensors for monitoring volcanoes in Japan detected up to the fifth passage of the wave circulating the Earth (Earthquake Research Institute 2022). Such atmospheric pressure pulses are brought by the Lamb wave (LW), a type of boundary wave that propagates along the Earth's surface with the sound speed (~ 0.3 km/s) (e.g., Kanamori et al. 1994).

In 1980 May, a VEI 5 eruption occurred at the volcano St. Helens, northwestern USA (~ 8000 km from Japan), and generated significant signals not only in atmospheric pressure, but also in ionosphere, being detected with two kinds of measurements, i.e., high-frequency (HF) Doppler sounding and the satellite Faraday rotation, at a few stations in the Kanto District, Japan (Ogawa et al. 1982). They inferred the propagation velocity of the ionospheric TEC (total electron content) anomalies comparing receiver records at three stations within the Kanto District and concluded that the disturbance propagated by ~ 0.291 km/s from the volcano. They suggested that the passage of LW from the volcano caused the atmospheric signals and that the energy leakage from troposphere to ionosphere caused the ionospheric signals.

The 1991 June VEI 6 eruption of the Pinatubo volcano, Philippines (~ 2500 km from Japan), caused long-period ionospheric fluctuations traveled northward with 0.3 km/s in Japan (Igarashi et al. 1994). Cheng and Huang (1992) also found ionospheric fluctuations with a period of 16–30 min traveling by 0.13–0.26 km/s in Taiwan and considered it the passage of internal gravity wave (IGW) excited by the Mt. Pinatubo eruption. In the 1980 and 1991 cases, however, small numbers and poor spatial coverage of sensors made it difficult to study the details of the disturbances.

Recent densifications of continuous global navigation satellite system (GNSS) receivers made it easy to monitor the Earth's ionosphere in terms of TEC, an integrated number of electrons along line-of-sights connecting satellites and receivers. Using such GNSS-TEC techniques, we detected ionospheric responses to large volcanic eruptions in Japan and in the world. They occur as harmonic oscillations of TEC (e.g., Nakashima et al. 2016; Shults et al. 2016; Shestakov et al. 2021; Heki and Fujimoto 2022), and as N-shaped short pulses of TEC changes (e.g., Heki 2006; Cahyadi et al. 2021), after

continuous Plinian eruptions and Vulcanian explosions, respectively. Both types of the disturbance signals propagate outward with a speed of 0.8–1.0 km/s, the acoustic wave velocity in the ionospheric F region. All these past GNSS-TEC studies are for near-field (within ~ 1000 km) disturbances caused by volcanic eruptions.

The 2022 Hunga Tonga-Hunga Ha'apai eruption is the first VEI 5 eruption that occurred after the worldwide deployment of numerous GNSS stations and has drawn lots of attention of researchers in this field. Soon after the eruption, GNSS stations in the Pacific Basin are reported to have caught significant ionospheric disturbances (JPL 2022). Then, Themens et al. (2022) reported that such disturbances were detected worldwide on the day of the eruption.

Here I investigate far-field ionospheric disturbances caused by this eruption using the dense GNSS array GEONET (GNSS Earth Observation Network) run by Geospatial Information Authority (GSI), Japan. The uniqueness of the present study includes: (1) comparison of the ionospheric and atmospheric signals both from dense ground sensor networks; (2) analyses of data on not only the eruption day, but also later days to study multiple passages of waves, and (3) utilization of a Japanese GNSS to analyze long continuous TEC records over days.

Atmospheric and ionospheric data

Atmospheric pressure

To study atmospheric signatures due to the 2022 Hunga Tonga-Hunga Ha'apai eruption, I use atmospheric pressure data from a dense array of weather sensors "Soratena", composed of ~ 1600 stations deployed by Weathernews Inc. throughout Japan (global.weathernews.com). Short-term enhancements of atmospheric pressure were recorded to pass over the Japanese Islands from SE to NW ~ 7 h after the eruption, together with smaller signals ~ 38 h after the eruption (Weathernews 2022). They indicate the passages of LW propagated from the volcano along the short-path (Fig. 1 inset), and the same wave after traveling round the Earth. In this study, I select 168 points uniformly distributed in Japan (Fig. 1) and analyze the 1-min sampling atmospheric pressure time series in Jan. 15–17 in local time (from Jan. 14, 15 UT to Jan. 17, 15 UT). These data shall be compared with the ionospheric disturbances recorded by GNSS stations.

Ionospheric TEC

Global Positioning System (GPS), the oldest GNSS, has been widely used for studying ionospheric TEC. GPS satellites employ orbital periods of a half sidereal day. Hence, they cannot stay above a reasonable elevation angle from a ground station longer than 4–5 h, and GPS-TEC data are composed of numerous short arcs. On the other hand, Quasi-Zenith Satellite System (QZSS), the Japanese satellite system for positioning, is composed of three satellites with quasi-zenith orbits (J01, J02, J03) and one geostationary orbit satellite (J07). These satellites stay longer within the view of Japanese stations (~ 8 and 24 h a day for J01-03 and J07, respectively). Especially, J07 enables us to observe TEC changes during the passages of air waves over Japan for days without disruptions.

I use QZSS raw data from GEONET. I use the whole set made of ~ 1500 points in drawing maps of ionospheric anomalies, but use a subset made of ~ 150 stations in drawing time series of wavelet transformed TEC anomalies. Line-of-sights to J07 are stationary and intersect the layer of maximum ionization (assumed at an altitude 300 km) of the ionosphere at points shifted a few hundreds of kilometers toward SSW from stations (Fig. 1). On the other hand, J01, J02, and J03 come in turn and stay around the local zenith for ~ 8 h a day so that we can monitor ionosphere just above stations with nearly vertical line-of-sights using either one of the three satellites. We converted the L1 and L2 carriers into slant TEC (STEC). STEC with J07 is converted to vertical TEC (VTEC) by multiplying with the cosine of the incidence angle of line-of-sight with the hypothetical thin layer at 300 km altitude. Basic procedures of the GNSS-TEC study follow Heki (2021).

Geomagnetic activities during this period were rather high, and the studied period (2022 Jan. 15–18) corresponds to the recovery phase from a geomagnetic storm that occurred on Jan. 14. The daily Kp index was in the range 2.0–3.3 during this period (omniweb.gsfc.nasa.gov).

Passages of the atmospheric waves

To isolate atmospheric signals associated with the LW passages, I approximate temporal variations of the pressure using polynomials and extract the departure from these reference curves as anomalies. Figure 2 gives four snapshots of their spatial distribution when the first LW passed over Japan. The signals look uniform throughout the country. The positive pressure anomalies lasting for ~ 20 min traveled from SE to NW with a speed of ~ 0.3 km/s.

The positive peak is as strong as ~ 1.5 hPa. We often observe brief but intense pressure changes in near-fields, such as the ~ 4.6 hPa pressure changes associated with the 2011 Jan. 31 eruption (VEI 2) of the Shin-Moe volcano, Kyushu, Japan (Cahyadi et al. 2021). Regarding the far-field pressure changes caused by LW from a distant volcano, Ogawa et al. (1982) reported one example, i.e., they observed ~ 0.1 hPa pressure change in Japan by the passage of LW excited by the 1980 St. Helens eruption (VEI 5). Considering the similar distance of the Hunga Tonga-Hunga Ha'apai and the St. Helens volcanoes from

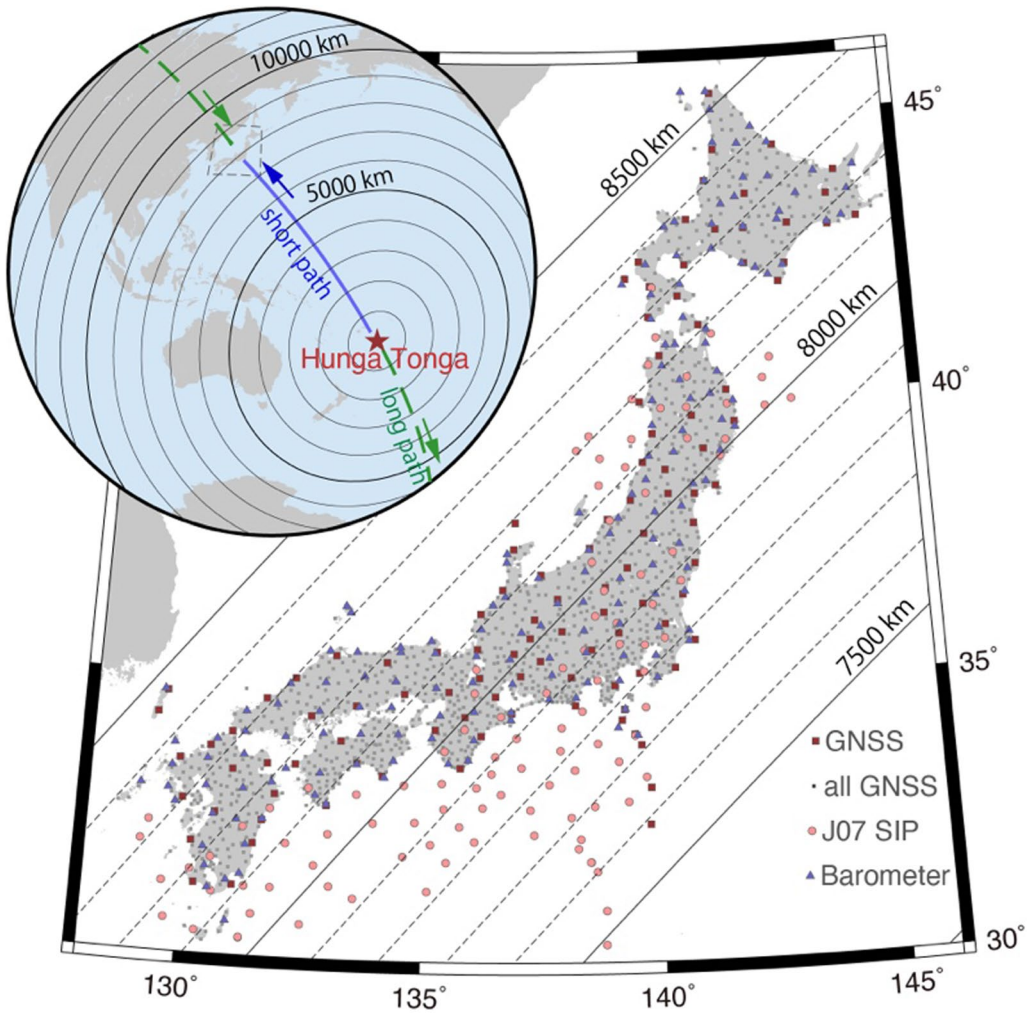

Fig. 1 Distribution of all (gray dots) and selected (dark red squares) GEONET GNSS stations, and selected Soratena weather sensor stations (triangles). Red circles indicate sub-ionospheric points (SIPs) for J07 (QZSS geostationary satellite). When we observe QZSS quasi-zenith orbit satellites (J01, 02, 03), SIPs stay close to the GNSS stations. Distances from the Hunga Tonga-Hunga Ha'apai volcano are indicated with black lines. The location of the volcano (red star), short and long paths from the volcano to Japan (blue and green curves) are given in the inset map

Japan (~8000 km), the difference in amplitudes would reflect the intensity contrast of the two eruptions.

Figure 3 shows the pressure anomalies as the function of time and distance from the volcano. The first passage of LW occurred 11–12 UT, Jan. 15, as seen in clear red colors along black dashed lines indicating the expected arrival times assuming 0.3 km/s propagation speed. In the close-up view (Fig. 3a), we can see numerous weaker waves follow the initial pulse. In contrast, there are no significant signals before the initial arrival of LW.

There seems to be another passage of a wave with a slower velocity at 14–15 UT (Fig. 3a), which might be the internal gravity wave (IGW). Their propagation velocity of ~0.225 km/s is close to the tsunami speed through an ocean as deep as 5200 m, and this IGW may have amplified the meteo-tsunami that hit Japanese coasts 3–6 h after the LW arrival (JAMSTEC 2022).

Here I define t indicating time in hour counted from the beginning of Jan. 15. The second passage of LW propagated along the long-path occurred ~8 UT on Jan. 16, i.e., $t = \sim 32$, as characterized by linear features with negative slopes. Its arrival times are earlier than expected by an hour (Fig. 3b). The second passage of IGW from NW to SE is expected $t = \sim 44$, but it seems to have occurred somewhat earlier, around $t = \sim 41$ (Fig. 3d). The third passage of LW from SE to NW is clearly seen at $t = 48$, early on Jan. 17, about a half hour earlier than expected.

Such differences in the arrival time are not due to the sphericity of the Earth. I calculate the distance between Japan and the volcano by approximating the Earth as a

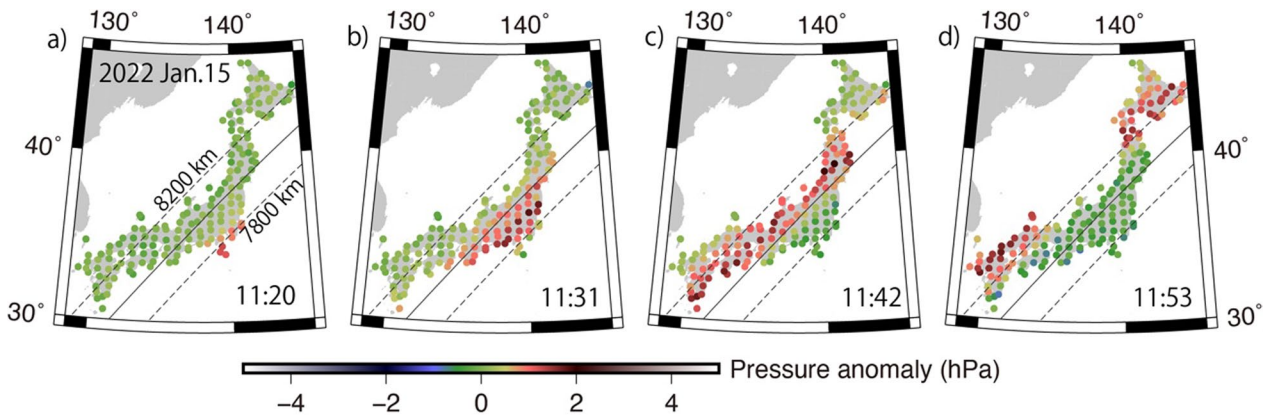

Fig. 2 The first passage of the LW on Jan. 15 shown with 4 snapshots from 11:20 to 11:53 UT. Atmospheric pressure anomaly, obtained as the deviation from best-fit polynomials, show the wavefront parallel to the distance contours and northwestward propagation as fast as ~ 0.3 km/s

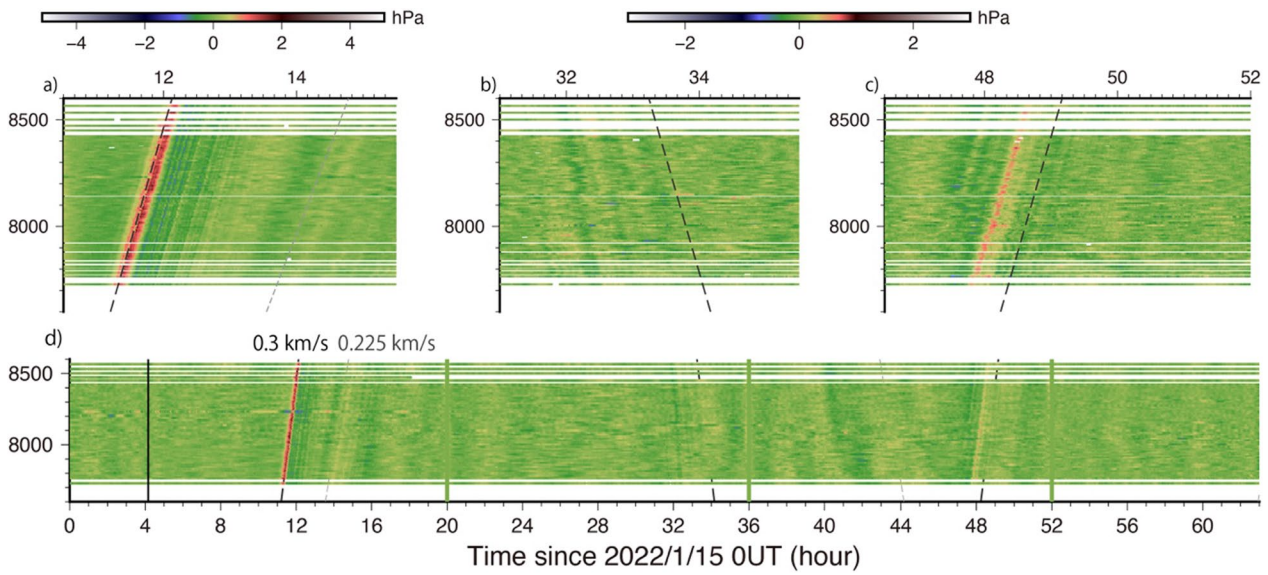

Fig. 3 Pressure anomalies as a function of time (horizontal axis) and the distance from the Hunga Tonga-Hunga Ha'apai volcano (vertical axis, unit km), obtained as residuals from best-fit degree-9 polynomials over the four time intervals (boundaries shown as thick vertical bars in green at 20, 36, and 52 h). The left and right color bars apply for **a**, **d** and **b**, **c**, respectively. The expected passage times calculated using the two velocities 0.300 km/s (LW) and 0.225 km/s (IGW) are indicated with thick and thin broken lines, respectively. The three panels in **a**–**c** show the close-up views of the time windows including the three passages of LW

sphere with the average radius (6371.012 km). The real short-path distance along the ellipsoid surface is somewhat shorter (e.g., vldb.gsi.go.jp/sokuchi/surveycalc/surveycalc/bl2stf.html), but the difference does not exceed 20 km. Differences in atmospheric structure (tropospheric temperature and sound velocity) and the wind system would have been responsible for these arrival time differences.

Passage of the ionospheric waves

TEC time series Jan. 15–18

Figure 4 shows continuous VTEC over four consecutive days observed with QZSS J07 at seven stations located along the LW propagation path. Superposed to diurnal changes, we can see strong positive pulses at 11–12 UT on Jan. 15. Their amplitudes are comparable to the background VTEC of ~ 10 TECU (TEC unit), where 1 TECU

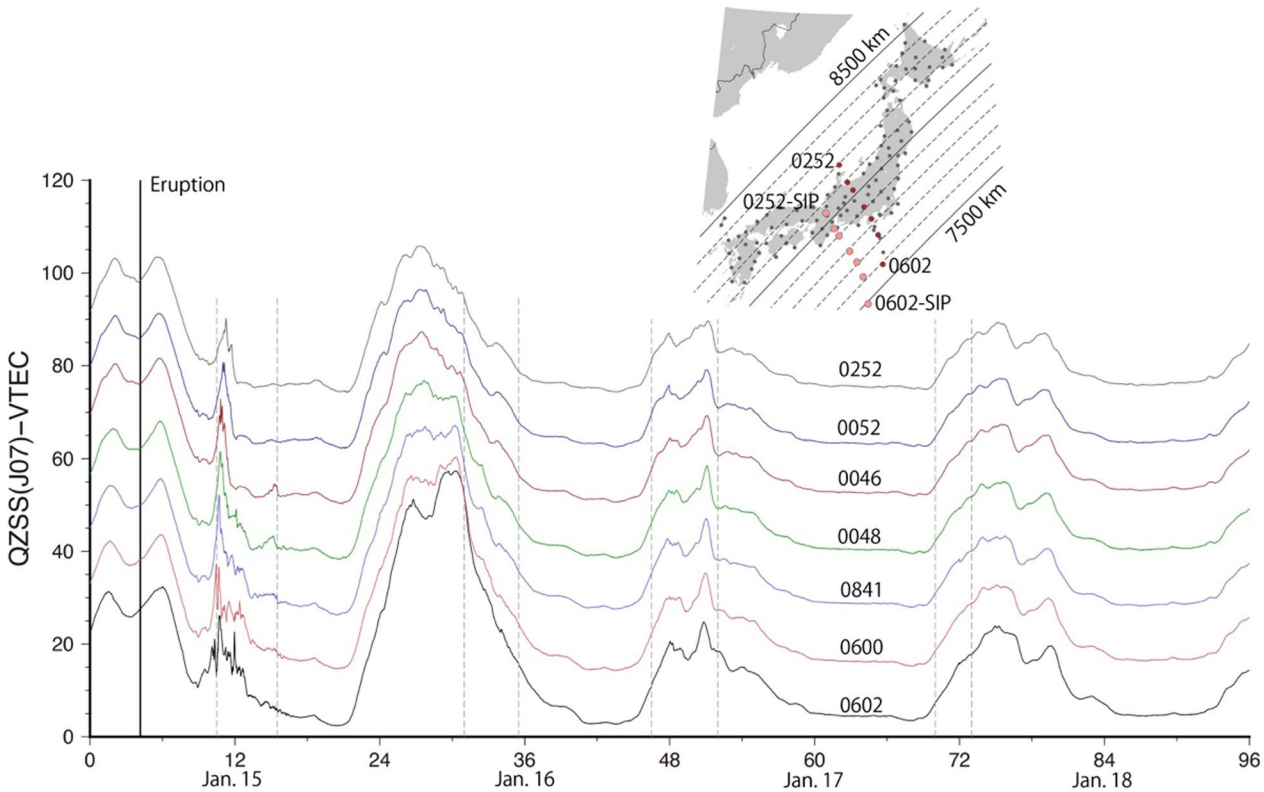

Fig. 4 VTEC time series at 7 GNSS stations (unit: TECU), located along the great circle from the Hunga Tonga-Hunga Ha'apai volcano, over 4 days (Jan. 15–18) observed using QZSS J07. Vertical plot biases of 12 TECU are given between VTEC curves to avoid overlaps of the curves. Numbers in the horizontal axis indicate *t*, hours from 0 UT on the first day. Vertical dashed lines indicate time windows shown in Fig. 6a–d. Inset map shows the locations of the 7 selected GNSS stations and their SIPs calculated assuming thin ionosphere as high as 300 km. The VTEC changes during the first LW passage ($t=7$–18) are magnified in Additional file 1: Fig. S1a

implies 10^{16} electrons/m^2. This amplitude is remarkable considering that the atmospheric pressure anomalies remain in the order of 1/1,000 of the background values. These initial anomalies arrive later for stations farther from the volcano reflecting the propagation of the anomalies from SE to NW (Additional file 1: Fig. S1).

The anomalies associated with the second LW passage around $t=32$–34 are not so clear as the first one because the passage occurred in the afternoon when the background TEC showed rapid monotonous decay ($t=30$–40). The anomalies appear as small undulations of the curves rather than clear peaks as seen in the first LW passage. Such undulations occur earlier at northern stations due to LW propagation from NW to SE. The anomalies associated with the third passage are recognized as weak and strong peaks around the noon of Jan. 17, $t=\sim 48$ and $t=\sim 50$, respectively. The occurrences of these peaks at the two ends have a time lag of ~ 0.5 h, corresponding to the time of LW propagating for ~ 600 km from SE to NW. Passage of the fourth wave of $t=\sim 72$ is not clear in VTEC time series.

Figures 2 and 3 show that atmospheric pressure signatures are quite uniform throughout Japan. On the other hand, Fig. 5 indicates that TEC signatures of the first LW passage are highly variable along the small circle with the same distance from the volcano (Additional file 1: Fig. S1b). For example, peaks are smaller, and the shapes are simpler in northeastern stations, e.g., 0019, than those in southwest, e.g., 0099. We can identify two peaks at 0165 and 0049 while only the earlier peak is clear at 0019 and 0054. Extremely strong disturbance at 0099 might include those by plasma bubbles considering that the local time is a few hours after sunset.

Detection of wave passages using wavelet

Because it is not easy to recognize the wave passages directly in VTEC plots (Figs. 4 and 5), I extract disturbance signals with a certain period (~ 30 min in this case) from TEC time series by wavelet transformation (Heki and Ping 2005). Figure 6e, f shows the results for J07 continuous VTEC records during Jan.15–18 at 42 stations

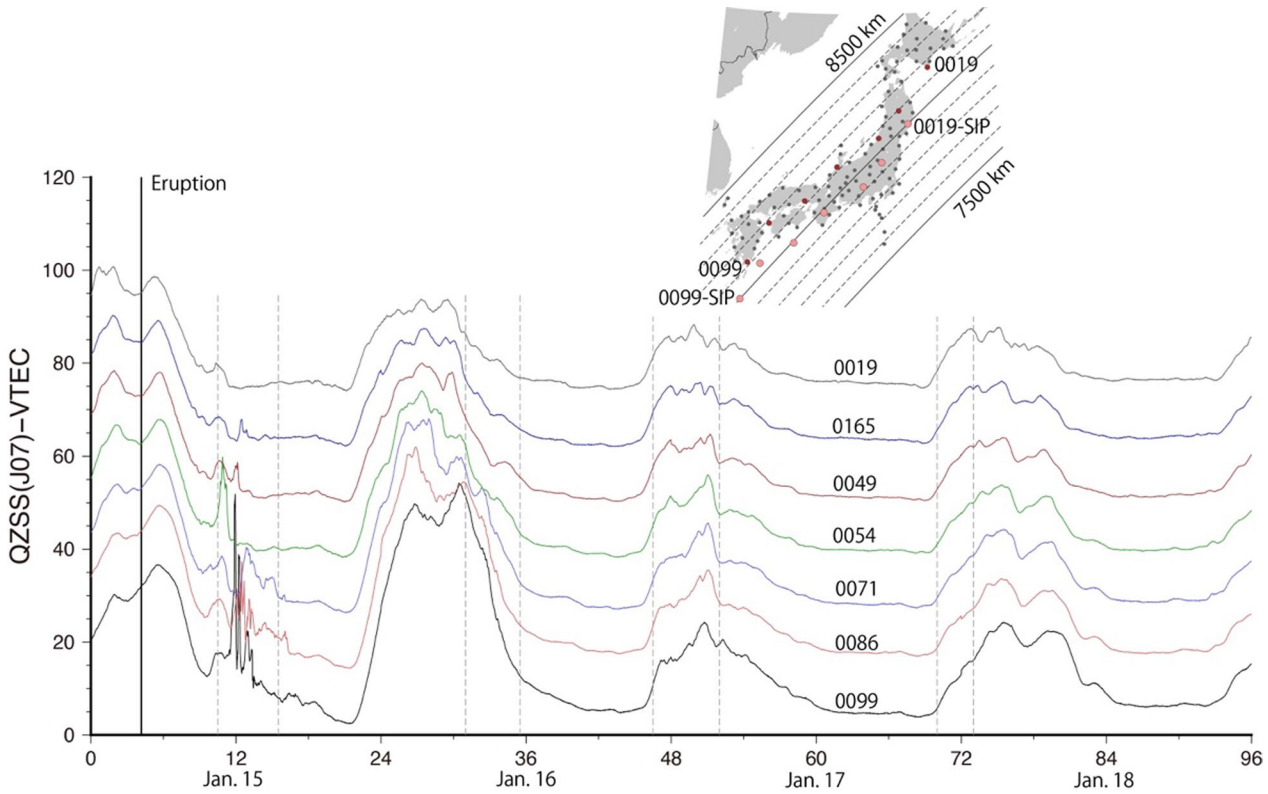

Fig. 5 VTEC time series at 7 GNSS stations, whose SIPs located along the small circle with the distance ~ 8000 km from the Hunga Tonga-Hunga-Ha'apai volcano. Shapes of the peaks associated with the first passage are diverse, e.g., one small/simple peak at 0019, two peaks at 0165/0049, and strong/complicated peaks at 0099. See Fig. 4 caption for details. The VTEC changes during the first LW passage ($t = 7$–18) are magnified in Additional file 1: Fig. S1b

selected as a subset of 150 stations, shown in Fig. 1, to avoid excessive overlaps of data. The J01–J03 data around the four passages of waves are magnified in Fig. 6a–d. Time windows of Fig. 6a–c are set identical to those in Fig. 3a–c (the atmospheric pressure data from SORATENA not available for the fourth passage).

Figure 6 is much noisier than the barometer data (Fig. 3). Nevertheless, we can recognize components traveling from SE to NW around $t = 12$–14 and $t = 48$–52, and from NW to SE around $t = 32$–34 and $t = 70$–72. The strength of four passage signals cannot be simply compared because they depend on background VTEC, which varies by an order of magnitude during a day (gray curves in Fig. 6e, f). For example, the first two passages occurred during evening hours when background VTEC is less than 10 TECU while the third and the fourth passages during daytimes. The fifth passage should be around $t = 84$–86, but Fig. 6f does not show any signatures for that.

There are several distinct differences in the ionospheric data (Fig. 6) from the barometer data (Fig. 3). An important difference is that significant ionospheric anomalies (Fig. 6a) seem to start well before the arrival of the pressure anomaly (Fig. 3a) by the LW passage. In Fig. 7, I mapped the VTEC anomalies during the first passage of LW. By comparing Figs. 2 and 7, one can notice that the passage of the TEC anomalies seems to have started significantly earlier than the LW arrival recorded as surface pressure variations. This will be discussed later.

Another prominent feature is the contrast in the disturbance amplitudes. Indeed, strong disturbances in Central Japan shown in Fig. 7 are overwhelming while the changes in other regions can be recognized only as subtle changes in the background color. Strong irregular changes in the southwesterly region may partly come from plasma bubble activities.

In the third passage, LW signatures are clear at $t = 48$–49 in barometer records (Fig. 3c). However, ionospheric signals at $t = 48$–49 are weaker than those at around $t = 50$–52.

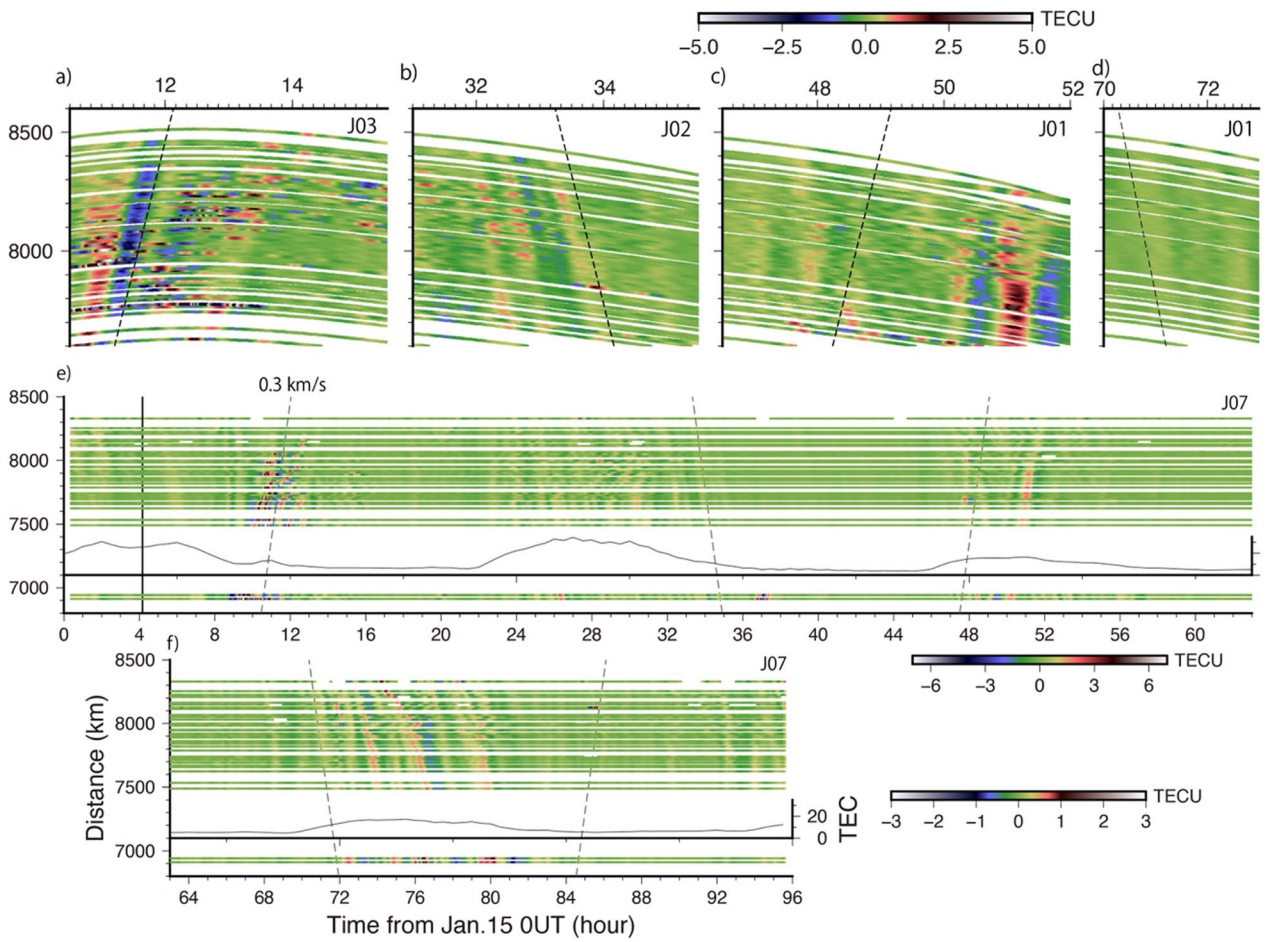

Fig. 6 Wavelet-transformed VTEC time series showing components with periods of ~ 30 min, using QZSS J07 (**e**, **f**) and J01–03 (**a**–**d**) data. Dashed lines indicate the expected passage times of a wave propagating with 0.3 km/s. **e** and **f** indicate the whole 4 days, while **a**–**d** show time windows around the LW passage times. Background VTEC, calculated at (35 N, 135E) using global ionospheric maps (GIM) (ftp.aiub.unibe.ch/CODE/), is shown as gray curves in **e** and **f**. Time and distance ranges of **a**–**c** are the same as those of Fig. 3a–c, but the distance range of **e** and **f** are wider than Fig. 3d

MSTID and mirror images of southern hemisphere disturbances

To interpret Fig. 6, it is important to distinguish the eruption-origin wave passage signatures from those by medium-scale traveling ionospheric disturbances (MSTIDs). In Fig. 6f, we recognize multiple clear stripes with negative slopes during Jan. 18 daytime (t=74–80). Here I demonstrate that these are the passage of winter daytime MSTIDs irrelevant to the Hunga Tonga-Hunga Ha'apai eruption.

A statistical study by Otsuka et al. (2011) showed that MSTIDs are classified into summer nighttime MSTID and winter daytime MSTID. The latter occurs as IGW and has nearly EW wavefronts and propagate southward by 0.1–0.2 km/s in Japan. In Jan. daytime, the occurrence rate of such MSTID exceeds 40%. Their signatures might be misinterpreted as the wave passages from NW to SE caused by the Hunga Tonga-Hunga Ha'apai eruption.

Additional file 1: Fig. S2 shows four snapshots of the positive and negative TEC anomalies around the noon, Jan. 18 (t=~75). Their wavefront strikes nearly EW, which is significantly different from the LW wavefront running NE–SW (Fig. 2). Moreover, their propagation speed is ~ 0.1 km/s, much slower than LW. Hence, stripes appearing on Jan. 18 daytime (Fig. 6f) would merely show MSTID irrelevant to LW from the volcano.

In contrast, the second passage (Fig. 6b) occurred late in the afternoon (t=32–33, corresponding 5–6 PM in local time), and it is unlikely that MSTID occurred at such local times (Otsuka et al. 2011). The fourth passage seen in Fig. 6d would not be due to MSTID, either, because it occurred early in the morning (t=70–71, corresponding to 7–8 AM in local time) when the occurrence probability of MSTID is still low.

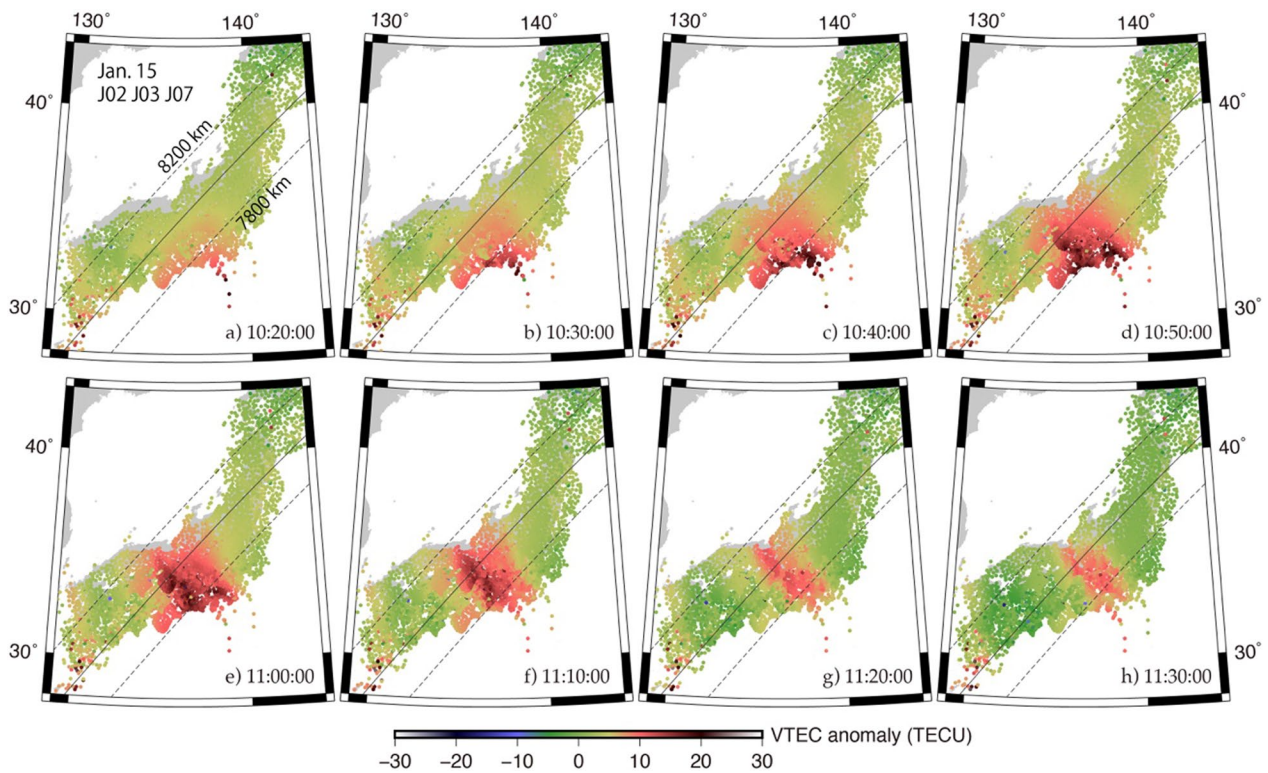

Fig. 7 Geographic distribution of the VTEC residuals at 8 epochs from Jan. 15, 10:20 UT (**a**) to 11:30 UT (**h**), from best-fit degree-4 polynomials estimated for $t = 7$–18 excluding the data within $t = 9$–14 (see Fig. S1 for the fit of such reference curves). I used all GNSS stations in Japan (small gray dots in Fig. 1) and three QZSS satellites J02, J03, and J07. The wavefront of the first LW passage is not so clear as Fig. 2 because of the existence of extremely large amplitude disturbances in Central Japan. The epoch of panel **g** corresponds to that of Fig. 2a

Lin et al. (2022) found that mirror images of the TEC anomalies by the Lamb wave propagating in southern hemisphere emerged simultaneously in the geomagnetic conjugate region in the northern hemisphere being coupled through geomagnetic field lines. Such conjugate anomalies appear in Japan when the Lamb wave propagates in the northern Australia from east to west. With a closer look into Additional file 1: Fig. S1, one may notice that small amount of TEC changes started as early as 8:30. They are the signatures of the conjugate anomalies of disturbances in northern Australia. In Additional file 1: Fig. S3, I plot TEC anomalies at four epochs in 8:30–9:00 UT. The figure clearly shows that the disturbance propagates westward at ~ 0.3 km/s with wavefronts parallel to the distance contour from the geomagnetic conjugate point of the volcano.

Relation between the ionospheric and the atmospheric waves

Two TEC peaks in the first passage and their arrival times

After the 1980 St. Helens eruption, Ogawa et al. (1982) compared the barometric and ionospheric signatures in Japan. However, they could not discuss precise time lags between them because the barometers and ionospheric SIPs are separated by > 200 km. Dense coverage of GNSS and barometers in the present case (Fig. 1) enables us to discuss exact time lags between the disturbances in the two spheres.

The VTEC anomalies propagate with the LW velocity of ~ 0.3 km/s for all the four passages (Fig. 6a–d). However, the occurrences of the strong peaks in TEC are not simultaneous with those of the Lamb pulses. Figure 8 compares the pressure and TEC changes in the same time windows at four positions, where the J07 SIPs of the GNSS stations and barometers nearly overlap. Figure 5 shows that the TEC disturbances are highly variable from place to place, and this is the case for these four stations. We recognize the existence of two peaks in Fig. 8a and d, the first peak (red arrow) comes ~ 40 min before the LW peaks and the second peak (blue arrow) occurs ~ 40 min later than the LW. The second peak is not always clear and is almost absent in Fig. 8b and c. This is irrelevant to the difference in the irregularity of the Earth's surface because their SIPs are located near the coast, that is, the

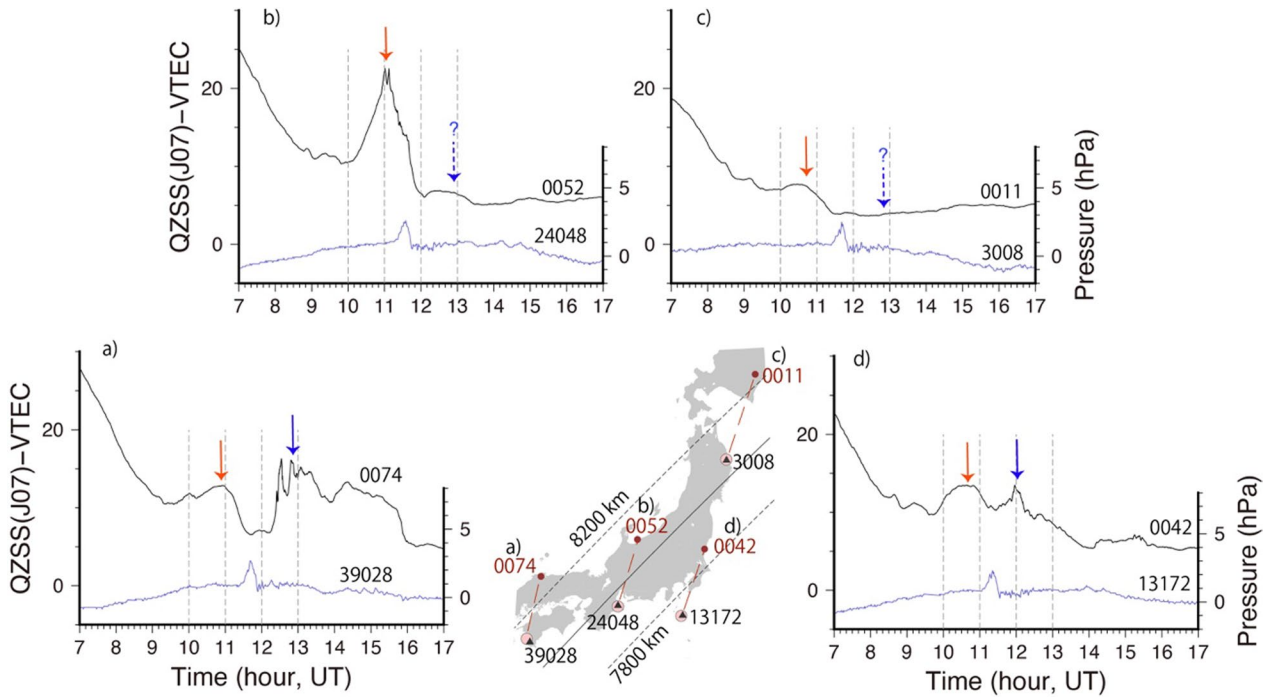

Fig. 8 Comparison of the pressure anomaly (blue) and VTEC (black) obtained using the geostationary satellite J07, on Jan. 15 around the first passage of LW. Positions of GNSS stations (red circles), their SIPs (pink circles), and barometers near SIPs (black triangles) are given in an inset map together with labels **a**–**d**. SIPs and corresponding GNSS stations are tied with red dashed lines. Two TEC peaks are evident for **a** and **d** (blue and red arrows), but only the first peak (red arrow) is clear in **b** and **c**. Vertical dashed lines are drawn for 10, 11, 12, 13 UT to facilitate the comparison of arrival times

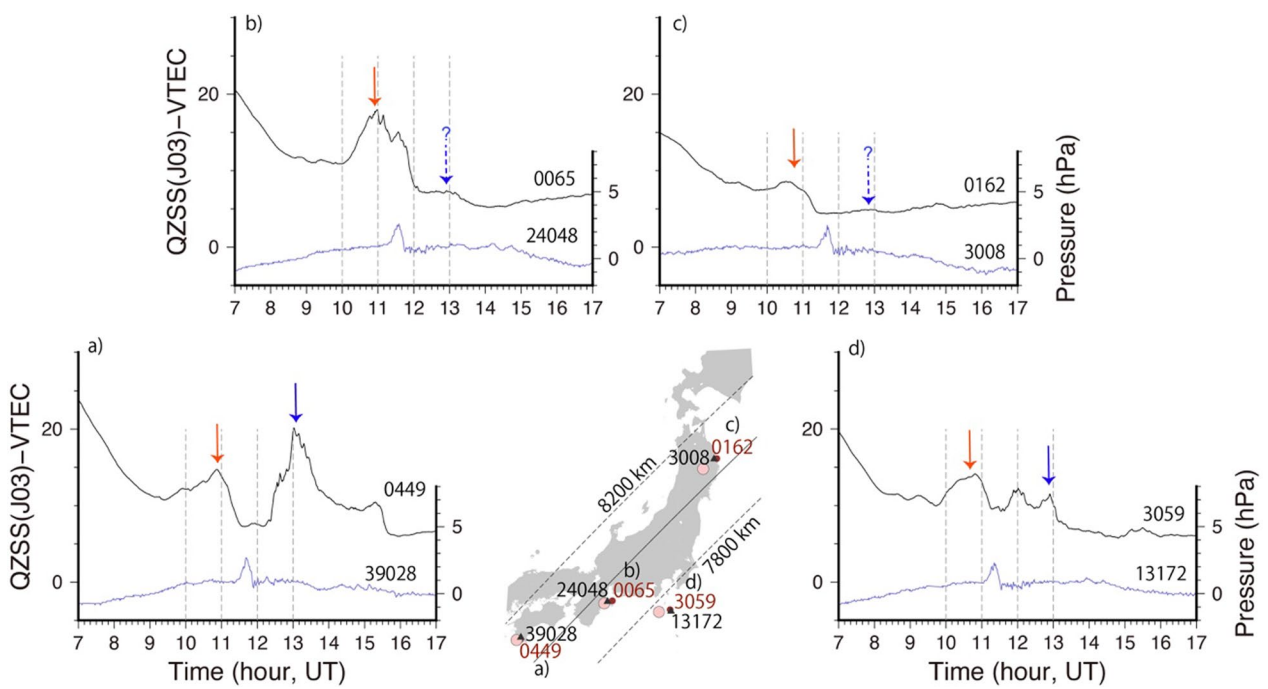

Fig. 9 Comparison of the pressure anomaly (blue) and VTEC (black) with the quasi-zenith orbit satellite J03, with nearly vertical line-of-sight, around the first passage of LW. Both the ground GNSS stations (red) and their SIPs at 11.7 UT (pink) are close to the barometers. See Fig. 8 caption for details

LW has travelled above flat ocean surface and just arrived at the coast in all these cases.

Figure 9 shows the VTEC changes at almost the same points in ionosphere as Fig. 8. I selected satellite J03, which was near zenith at that time, and plotted VTEC using GNSS stations close to the barometers. Although SIP positions in Fig. 8 depend on the assumed ionospheric height, those in Fig. 9 are free from such uncertainties (the line-of-sights are nearly vertical). VTEC shown in Figs. 8 and 9 are similar, suggesting that the height 300 km assumed in calculating SIPs was appropriate. At the same time, they show subtle differences especially around sharp peaks of TEC anomalies, possibly due to complex spatial structures of the electron density anomalies. Nevertheless, existence of the two peaks in (a) and (d) and absence of the second peak in (b) and (c) are common in Figs. 8 and 9.

Origins of the two TEC peaks

Although the emergences of the first TEC peaks are earlier than the LW arrivals (Figs. 8 and 9), its propagation velocity is consistent with the LW velocity of ~ 0.3 km/s (Fig. 6). Thus, the ionospheric disturbance would be a secondary feature made by energy leakage from the atmospheric LW. This is also supported by HF Doppler observations after the 1980 St. Helens eruption. Ogawa et al. (1982) found a subtle phase lag of a few minutes between the HF Doppler records with two different frequencies (5 and 8 MHz) and considered that the phase lag reflects the upward propagation of the disturbance. Here, I assume that ionospheric disturbances are caused by upward energy leakage from LW propagating through the Earth's troposphere.

Interpretation of the backward energy leakage, i.e., TEC changes occurring after the passage of pressure waves, is straightforward. IGW excited by LW would reach the ionospheric F region and disturb the TEC in 20–30 min. TEC peaks occurring after the LW passage in Figs. 8 and 9 would originate from such atmospheric waves.

In contrast, forward energy leakage, i.e., the TEC increases occurring ~ 40 min prior to the first LW arrival (Figs. 8 and 9), seems enigmatic (such forward leakage is not seen in the second and the third LW passages). The acoustic wave (AW) velocity in ionosphere is much faster (~ 1 km/s in F region) than LW. Hence, if LW excites significant amplitudes of upgoing AW, a part of the refracted AW may overtake and lead the LW wavefront. However, LW is essentially hydrostatic in vertical, and it is not conceivable that it excites significant AW (e.g., Gill 1982). In fact, the extension of Lamb wave in thermosphere occurs as IGW rather than AW (Lindzen and Blake 1972). Consequently, the emergence of upper altitude disturbances occurs later than the disturbance in lower altitudes (Sharman et al. 1988). Nevertheless, Figs. 7, 8, 9 demonstrate that ionospheric disturbances preceded the first LW arrivals on the surface on Jan. 15. I wish this paradox will be clarified in the future.

Conclusions

I summarize this study as follows:

1. The 2022 Jan. 15 eruption of the Hunga Tonga-Hunga Ha'apai submarine volcano excited Lamb waves that traveled round the Earth several times as fast as ~ 0.3 km/s.
2. I compared the atmospheric pressure signals with the disturbance signatures in ionospheric TEC using the QZSS satellites observed by the dense GNSS array in Japan.
3. Ionospheric disturbances traveled as fast as the Lamb wave, suggesting its secondary origin, i.e., the upward energy leakage from lower troposphere.
4. Although the atmospheric pressure disturbances remained of the order of 1/1,000 of the background values, TEC often showed disturbances with amplitudes comparable to the background values. The amplitudes and the waveforms were highly variable along the wavefront.
5. Ionospheric disturbances started ~ 40 min before the initial arrival of the Lamb wave, which is not well understood by our current knowledge.

Abbreviations

AW: Acoustic wave; GEONET: GNSS Earth Observation Network; GNSS: Global navigation satellite system; GIM: Global Ionospheric Map; GPS: Global Positioning System; GSI: Geospatial Information Authority of Japan; HF: High frequency; IGW: Internal gravity wave; LW: Lamb wave; MSTID: Medium scale traveling ionospheric disturbance; QZSS: Quasi-Zenith Satellite System; SIP: Sub-ionospheric point; STEC: Slant TEC; TEC: Total electron content; TECU: TEC unit; UT: Universal Time; VEI: Volcanic explosivity index; VTEC: Vertical TEC.

Supplementary Information

The online version contains supplementary material available at https://doi.org/10.1186/s40623-022-01674-7.

Additional file 1. Three auxiliary figures (Figure S1, S2, and S3) are given as the supplementary material. These figures are all quoted in the main text.

Acknowledgements

The Soratena barometer data have been provided by courtesy of Weathernews Inc.. The GEONET GNSS raw data files can be downloaded from Geospatial Information Authority of Japan website (terras.gsi.go.jp). I thank two anonymous reviewers for constructive and thoughtful comments.

Author contributions

KH: conceptualization, data analysis, writing manuscript. The author read and approved the final manuscript.

Authors' information
Kosuke Heki is a professor emeritus in Department of Earth and Planetary Sciences, Hokkaido University, Japan, and a visiting professor at Chinese Academy of Sciences, Shanghai Astronomical Observatory. He studies space geodesy, with strong interest in atmospheric sensing with GNSS. He pioneered various applications of GNSS-TEC including ionospheric disturbances immediately before and after large earthquakes.

Funding
This research was supported by JSPS KAKENHI Grant number JP20K04120. The author is also supported by Chinese Academy of Sciences, President's International Fellowship Initiative (Grant number 2022VEA0014).

Availability of data and materials
GEONET data can be downloaded from GSI ftp server (terras.gsi.go.jp) after a simple registration procedure. The Soratena atmospheric pressure data can be obtained by writing to Weathernews Inc. (global.weathernews.com/news/16551). A basic set of the software systems used in this study can be found in the web page of the author (www.ep.sci.hokudai.ac.jp/~heki/software.htm).

Declarations

Competing interests
The author declares that he has no known competing financial interests or personal relationships that could have appeared to influence the work reported in this paper.

Author details
[1]Shanghai Astronomical Observatory, Chinese Academy of Sciences, 80 Nandan Rd., Shanghai 200030, China. [2]Department of Earth and Planetary Sciences, Hokkaido University, N10 W8, Kita-ku, Sapporo, Hokkaido 060-0810, Japan.

Received: 14 March 2022 Accepted: 5 July 2022
Published online: 20 July 2022

References

Cahyadi MN, Handoko EY, Rahayu RW, Heki K (2021) Comparison of volcanic explosions in Japan using impulsive ionospheric disturbances. Earth Planets Space 73:228. https://doi.org/10.1186/s40623-021001539-5
Cheng K, Huang YN (1992) Ionospheric disturbances observed during the period of Mount Pinatubo eruptions in June 1991. J Geophys Res 97(A11):16995. https://doi.org/10.1029/92JA01462
Earthquake Research Institute (2022) Volcanic activity of Hunga Tonga Hunga Ha'apai underwater volcano. www.eri.u-tokyo.ac.jp/en/news/4824/
Gill AE (1982) Section 6.2, The case of two superposed fluids of different density, from "Atmosphere-Ocean Dynamics", International Geophysics Series 30:119–127, Academic Press, San Diego
Heki K (2006) Explosion energy of the 2004 eruption of the Asama Volcano, central Japan, inferred from ionospheric disturbances. Geophys Res Lett 33:L14303. https://doi.org/10.1029/2006GL026249
Heki K (2021) Chapter 21: Ionospheric Disturbances Related to Earthquakes in Ionospheric Dynamics and Applications. Geophysical Monograph 260, edited by C. Huang and others, pp. 511–526, Wiley/American Geophysical Union, https://doi.org/10.1002/9781119815617.ch21
Heki K, Fujimoto T (2022) Atmospheric modes excited by the 2021 August eruption of the Fukutoku-Okanoba volcano, Izu-Bonin Arc, observed as harmonic TEC oscillations by QZSS. Earth Planets Space 74:27. https://doi.org/10.1186/s40623-022-01587-5
Heki K, Ping J-S (2005) Directivity and apparent velocity of the coseismic ionospheric disturbances observed with a dense GPS array. Earth Planet Sci Lett 236:845–855. https://doi.org/10.1016/j.epsl.2005.06.010
Igarashi K, Kainuma S, Nishimuta I, Okamoto S, Kuroiwa H, Tanaka T, Ogawa T (1994) Ionospheric and atmospheric disturbances around Japan caused by the eruption of Mount Pinatubo on 15 June 1991. J Atmos Terr Phys 56(9):1227–1234. https://doi.org/10.1016/0021-9169(94)90060-4
JAMSTEC (2022) On the atmospheric and oceanographic variations associated with the large eruption. www.jamstec.go.jp/j/jamstec_news/tonga/column03/. **(in Japanese)**
Jet Propulsion Laboratory (2022) Tonga eruption sent ripples through earth's ionosphere. www.jpl.nasa.gov/news/tonga-eruption-sent-ripples-through-earths-ionosphere
Kanamori H, Mori J, Harkrider DG (1994) Excitation of atmospheric oscillations by volcanic eruptions. J Geophys Res 99:21947–21961
Lin J-T, Rajesh PK, Lin CC-H, Chou M-Y, Liu J-Y, Yue J, Hsiao T-Y, Tsai H-F, Chao H-M, Kung M-M (2022) Rapid conjugate appearance of the giant ionospheric Lamb wave signatures in the northern hemisphere after Hunga-Tonga volcano eruptions. Geophys Res Lett. https://doi.org/10.1029/2022GL098222
Lindzen RS, Blake D (1972) Lamb waves in the presence of realistic distributions of temperature and dissipation. J Geophys Res 77:148–227. https://doi.org/10.1029/JC077i012p02166
Nakashima Y, Heki K, Takeo A, Cahyadi MN, Aditiya A, Yoshizawa K (2016) Atmospheric resonant oscillations by the 2014 eruption of the Kelud volcano, Indonesia, observed with the ionospheric total electron contents and seismic signals. Earth Planet Sci Lett 434:112–116. https://doi.org/10.1016/j.epsl.2015.11.029
Ogawa T, Kumagai H, Sinno K (1982) Ionospheric disturbances over Japan due to the 18 May 1980 eruption of Mount St. Helens. J Atmos Terr Phys 44:863–868
Otsuka Y, Kotake N, Shiokawa K, Ogawa T, Tsugawa T, Saito A (2011) Statistical study of Medium-Scale Traveling Ionospheric Disturbances observed with a GPS receiver network in Japan. In: Abdu MA, Pancheva D, Bhattacharyya A (eds) Aeronomy of the Earth's Atmosphere and Ionosphere, vol 291. IAGA Special Sopron Book Series 2
Sharman RD, Keller TL, Wurtele MG (1988) Incompressible and anelastic flow simulations on numerically generated grids. Monthly Weather Rev 116:1124–1136. https://doi.org/10.1175/1520-0493(1988)116
Shestakov N, Orlyakovskiy A, Perevalova N, Titkov N, Chebrov D, Ohzono M, Takahashi H (2021) Investigation of ionospheric response to June 2009 Sarychev peak volcano eruption. Remote Sens 13:648. https://doi.org/10.3390/rs13040638
Shults K, Astafyeva E, Adourian S (2016) Ionospheric detection and localization of volcano eruptions on the example of the April 2015 Calbuco events. J Geophys Res Space Phys 121:10303–10315. https://doi.org/10.1002/2016JA023382
Themens RT, Watson C, Žagar N, Vasylkevych S, Elvidge S, McCaffrey A, Prikryl P, Wood A, Jayachandran PT (2022) Global propagation of ionospheric disturbances associated with the 2022 Tonga volcanic eruption. Geophys Res Lett. https://doi.org/10.1029/2022GL098158
Weathernews (2022) Sudden changes in atmospheric pressure due to shockwaves from Tonga volcanic eruption observed. global.weathernews.com/news/16551

Publisher's Note